Loss spectrum measurement for infrared hollow fiber based on the Fourier transform infrared spectrometer

Cong-Hui Yang,[1] Hua Hua,[1] Wei Tan,[1] Katsumasa Iwai,[2] Mitsunobu Miyagi,[2] Nan Chi,[1] and Yi-Wei Shi[1,*]

[1]School of Information Science and Engineering, Fudan University, 220 Handan Road, Shanghai 200433, China

[2]Sendai National College of Technology, Sendai 989-3128, Japan

*Corresponding author: ywshi@fudan.edu.cn

Received 16 February 2010; accepted 30 March 2010; posted 7 April 2010 (Doc. ID 124332); published 26 April 2010

Based on the Fourier transform infrared spectrometer, a system for measuring the loss spectrum of hollow fiber is established. Loss spectra can be measured for hollow fibers with length ranging from several centimeters to 3 m. Two kinds of light source coupler are designed and fabricated for achieving stable coupling and a repeatable spectrum. One is a short waveguide, and the other is a tapered tube. Both are inner-coated with a silver layer and they are of the same inner diameter at the output end as the measured hollow fiber. Characteristics of the measuring system are discussed theoretically and experimentally when using the two couplers. Several kinds of hollow fibers are measured, and the properties of the loss spectra are discussed. The measured loss value is shown to be dependent on the output divergence angle of the coupler. The tapered coupler has a larger output divergence and causes higher measured loss than that of the waveguide coupler. © 2010 Optical Society of America

OCIS codes: 230.7370, 310.6860, 120.7000, 060.2270, 120.6200.

1. Introduction

Infrared hollow fiber has found applications [1–3] in medical, industrial, and sensing fields due to its advantages of simple structure, low loss, and high laser-induced-damage threshold. Hollow fibers can be grouped into two categories: those with inner wall materials that have a refractive index n of less than 1, and those with inner wall materials whose n is greater than 1. The leaky hollow fibers [4], with $n > 1$, have metallic and dielectric films deposited on the inner surface of a capillary. The attenuated total reflection (ATR) [5] hollow fibers are made of some special $n < 1$ oxide glasses. ATR hollow fibers may include GeO_2 coated [6] hollow fibers and hollow sapphire fibers [7]. GeO_2 fibers are fabricated by depositing GeO_2 film inside glass tubing. Hollow sapphire fibers are single-crystal fibers grown by the laser-heated pedestal growth method. The dielectric/metal coated hollow fibers are normally fabricated by using liquid-phase coating techniques and depositing metallic and dielectric coating inside capillary tubing.

Loss spectra of hollow fibers show the properties of film material absorptions and interference peaks and valleys. These properties in the loss spectra provide important information for optimizing the fiber fabrication, such as film material selection and the thickness of the inner coating films. By using the low-loss fiber as a sensing probe, the loss spectrum can be measured for gas absorption, reflection, and transmission properties of materials or gases. The positions and strength of the absorption peaks are related to the material ingredients and their concentration. Endoscopic measurement and laser treatment are

0003-6935/10/132504-06$15.00/0

applications that are based on the low-loss properties and high-power capability both in the mid- and far-infrared wavelength regions of the hollow fibers.

We used the Fourier transform infrared (FT-IR) spectrometer to establish a measuring system of hollow fiber for the loss spectrum in the mid-infrared (MIR) region. The dielectric/metal-coated hollow fibers, GeO_2 coated hollow fibers and hollow sapphire fibers, were measured by using the system. A repeatable spectrum was obtained for the hollow fibers. Theoretical calculations were also conducted for the above-mentioned fibers according to the loss theory of circular hollow fibers.

2. Measuring System

Figure 1 shows the optical diagram of an FT-IR. The optical reflections shown by the dashed lines were the original optical transmission before FT-IR modification. The sample compartment is about 20 cm long. It is difficult to measure a sample longer than the compartment. To measure the loss property of infrared hollow fiber, the beam was guided out of the FT-IR spectrometer through the infrared window by the reflector at the center. The beam was focused by an elliptical mirror and coupled into a coupler. The output energy of the coupler and measured fiber were measured by the external detector. The elliptical mirror and the coupler were fixed on the external optical platform. With an external detector, a sample compartment was built up. The measuring system can measure fibers with lengths from several centimeters to several meters.

The coupler is one of the most important components. It has great influence on the coupling efficiency and measured attenuations. We designed and fabricated two kinds of coupler for the system. One is a silver-coated hollow waveguide coupler. The other is a silver-coated hollow tapered coupler [8]. The inner diameter at the output end is the same as the measured fiber for both couplers. This helps to achieve the stability of coupling efficiency. Figure 2 shows pictures of the two couplers and their expected focusing

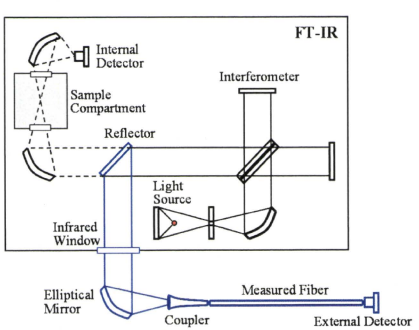

Fig. 1. (Color online) Schematic diagram of the measuring system.

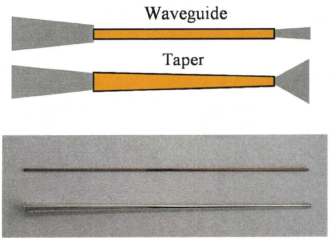

Fig. 2. (Color online) Pictures and focus images for a waveguide coupler and a tapered coupler.

properties. The tapered coupler accepts more energy because of its larger bore size at the input end. This results a good coupling efficiency. On the other hand, a tapered coupler may cause a larger divergence angle for the output light. It excites more higher-order modes with high propagation losses in the fiber.

Two kinds of hollow fiber were selected as the samples for the test measurement. They were inner coated with films of AgI/Ag [9] and OC300/Ag [10]. As shown in Fig. 3, loss spectra were measured with both couplers for the two fibers. Figure 4(a) is the loss spectra for AgI/Ag-coated hollow fiber. The length of the fiber is 1107 mm and the inner diameter is 0.7 mm. The loss peak at a 2 μm wavelength is caused by the interference of light in the thin AgI film. Peaks

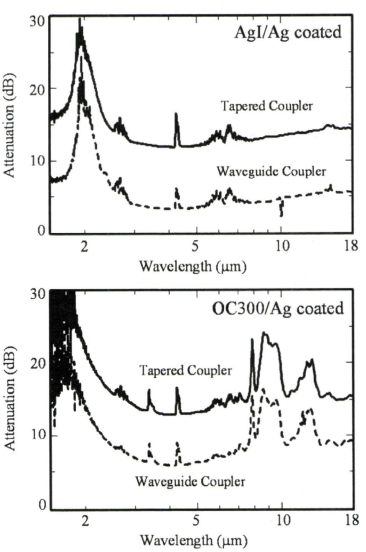

Fig. 3. Measured loss spectra of leaky infrared hollow fibers using different couplers.

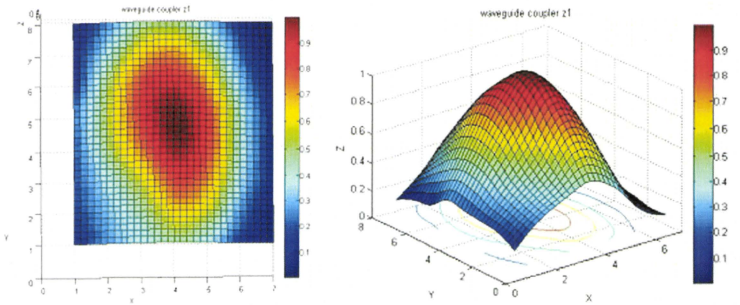

Fig. 4. (Color online) Light intensity distribution at the output end of the fiber coupler. (a) Plane Z_1 and (b) plane Z_2 were 1.5 and 3 mm from the output end, respectively.

at wavelength bands of 4.3 and 6 μm are caused by the absorption of CO_2 gas and water vapor in the air. Figure 3(b) is the loss spectra of OC300/Ag-coated hollow fiber. The length of the fiber is 785 mm and the inner diameter is 0.7 mm. Peaks at the wavelength band of 3.5 and 8–13 μm are caused by the intrinsic absorption of the OC300 film. Fibers were measured several times in a few days. A repeatable loss spectrum was obtained for both couplers. However, we note that the spectrum has different attenuation values even for an identical fiber when using different couplers.

3. Discussion

Analysis indicated that the attenuation of hollow fiber is dependent on the coupling conditions of the light source [11]. A larger divergence angle will excite more higher-order modes, which causes higher loss. We measured the divergence angles at the output ends of both couplers. Take two normal planes at the output end of the coupler and scan the light intensity. Figure 4 shows the two- and three-dimensional intensity distributions at the planes Z_1 and Z_2, which were 1.5 and 3 mm from the output end. We obtained full width at half-maximum (FWHM) of light at each plane according to the distribution. The divergence angle of the light can be calculated by using the two FWHM values and the distance between the normal planes. Measurement results showed that the divergence angle was dependent on the length of the coupler. When the waveguide-type coupler has a length of 120 mm, the divergence angle was 9.7° along the X axis and 19.5° along the Y axis. The light intensity showed an approximately Gaussian distribution. It means that most energy was in a low-order mode. The same measurements were made on the tapered coupler. The light intensity distribution is shown in Fig. 5 and the divergence angles were 16° and 98° along the X axis and the Y axis, respectively. As lots of high-order modes exist, the distribution shows several high-intensity spots. Moreover, intensity distributions for both couplers were elliptical because of the properties of the light source. The MIR light source of FT-IR is a globar, a heated silicon carbide rod.

The transmitted power $P(z)$ in hollow fibers can be expressed as [12]

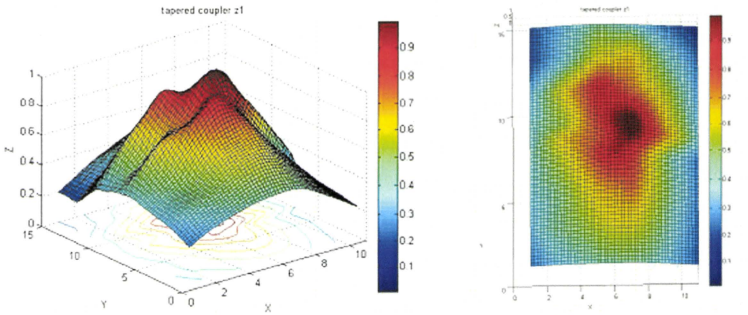

Fig. 5. (Color online) Light intensity distribution at the output end of the tapered coupler.

$$P(z) = \int_0^{\theta_{\max}} p(\theta_z) \exp\{-[1 - R(\theta_z)]z/2T \cot\theta_z\} \sin\theta_z \mathrm{d}\theta_z, \quad (1)$$

where $\theta_{\max}$ is the maximum launching angle, $p(\theta_z)$ is the angular distribution of the launching power, $R(\theta_z)$ is the power reflection coefficient of the light, and T is the inner diameter of the fiber. By taking into consideration the divergence angle, the film thickness, and surface roughness, we obtained the calculated result for the loss spectrum.

A cyclic olefin polymer (COP)/Ag-coated hollow fiber [13] was used for the comparison of calculated and measured spectra. The fiber is 1003 mm long, with a 0.7 mm inner diameter. The calculated and measured loss spectra using different couplers are shown in Fig. 6. Peaks at the wavelengths of 2 and 4 μm are caused by the interference of light in the thin COP film. Sharp peaks at 3.5 and 7 μm are caused by the absorption of the COP. In the spectrum calculation, film thickness, film surface roughness, and the beam divergence angle were adjusted to match the measured results. Calculation results showed that the COP film thickness was 0.85 μm and the surface roughness was 30 nm in root mean square (rms). The divergence angles in the calculation were 15° and 45° for the waveguide coupler and the tapered coupler, respectively. Considering the influence of an elliptical intensity distribution of the light beam (in the calculation, the intensity was assumed to be of circular distribution), the results agree well with the measured results. The divergence angles used in the calculation were reasonable. The absorption peaks at the wavelengths of 3.5 and 7 μm disappeared in the calculated spectra because we did not take into consideration the material absorption for the polymer layer in the calculation.

We also made the calculation and measurement for two ATR-type hollow fibers, GeO_2 coated hollow glass fiber and hollow sapphire fibers. The GeO_2 fiber is 300 mm long and 1.4 mm in inner diameter. Figure 7 shows the loss spectra for measured and calculated results. Low-loss windows can be found at the wavelength bands of 7.6 and 10–12 μm. These low-loss wavelength bands are caused by the properties of the materials of the base tube (SiO_2) and inner-coated film (GeO_2). The inset in Fig. 7 shows the loss spectra for the glass-based tube. The refractive index n is less than 1 for SiO_2 around 7.6 μm. n of GeO_2 is less than 1 around 10–12 μm. Sol-gel GeO_2 coatings were deposited into silica glass substrate

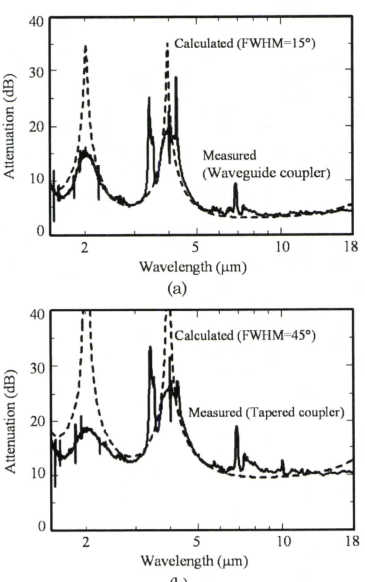

Fig. 6. Calculated and measured loss spectra using (a) the waveguide coupler and (b) the tapered coupler.

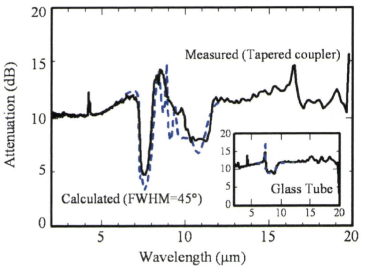

Fig. 7. (Color online) Calculated and measured loss spectra for a GeO_2 coated hollow glass fiber.

by cycles of a dip-coating operation. Since the thickness of a single layer of GeO_2 produced in this way was typically limited to less than 0.4 μm, several cycles were needed to build up uniform thick coatings. According to the fabrication parameters, the GeO_2 film was of 2.8 μm thickness in the theoretical calculation. The surface roughness was 80 nm in rms. Loss peaks in calculation results at 8.9 and 9.4 μm were caused by the multilayered film antireflection. Sharp antireflection peaks disappeared in the measured loss spectrum. This is because the accumulated thick GeO_2 film has a rather rough surface. The hollow sapphire fiber, a product of Saphikon, Inc., has a length of 990 mm and an inner diameter of 1 mm. Figure 8 shows the loss spectra. The low-loss area was found from 10 to 17 μm. This is because the refractive index n of Al_2O_3 is less than 1 in the wavelength band. In the calculation, the divergence angle is 45°.

We note that the theoretical loss spectra are in good accordance with the measured results both in low-loss wavelength bands and the absorption peaks in Figs. 7 and 8. This means that the measured spectrum from the system is reliable. Furthermore, both the ATR fibers have a low-loss property around 10.6 μm, which makes them suitable for delivering CO_2 laser light. The data of refractive indices for

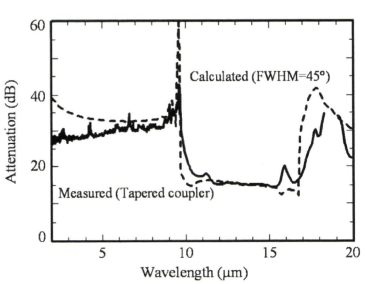

Fig. 8. Calculated and measured loss spectra for a hollow sapphire fiber.

GeO_2, SiO_2, and Al_2O_3 (sapphire) used in the calculations are taken from published literature [14,15].

4. Conclusions

Based on a commercially available FT-IR spectrometer, a beam was guided out of the FT-IR and a new sample compartment was built on the optical platform with an external detector. The loss spectra of hollow fibers with lengths ranging from several centimeters to 3 m can be measured. We designed and fabricated two couplers, a waveguide coupler and a tapered coupler, to achieve repeatable spectrum and easy coupling. The attenuation values changed when different couplers were used, even for the identical fiber, because of the influence of the divergence angle of the incident light source. The experimental and theoretical results are helpful in the improvement of the coupling methods of the infrared spectrum measuring system and the design of infrared fiber sensors.

This research is financially supported by the National Natural Science Foundation of China (NSFC) (60971014), the National Basic Research Program of China (2010CB328300), and the 211 Project for construction of key disciplines, as well as by the Health and Labor Science Research Grants (H20-nano-young-010), Japan.

References

1. M. Mohebbi, "Transmission characteristics of femtosecond optical pulses in hollow-core fibers," Opt. Commun. **253**, 290–300 (2005).
2. S. Sato, Y. W. Shi, Y. Matsuura, M. Miyagi, and H. Ashida, "Hollow waveguide based nanosecond, near-infrared pulsed laser ablation of tissue," Lasers Surg. Med. **37**, 149–154 (2005).
3. S. S. Kim, N. Menegazzo, C. Young, J. Chan, C. Carter, and B. Mizaikoff, "Mid-infrared trace gas analysis with single-pass Fourier transform infrared hollow waveguide gas sensors," Appl. Spectrosc. **63**, 331–337 (2009).
4. M. Miyagi and S. Kawakami, "Design theory of dielectric-coated circular metallic waveguides for infrared transmission," J. Lightwave Technol. **2**, 116–126 (1984).
5. C. C. Gregory, and J. A. Harrington, "Attenuation, modal, and polarization properties of $n < 1$, hollow dielectric fibers," Appl. Opt. **32**, 5302–5309 (1993).
6. C. B. Jing, J. X. Hou, and X. G. Xu, "Fabrication and optical characteristics of thick GeO_2 sol-gel coatings," Opt. Mater. **30**, 857–864 (2008).
7. R. K. Nubling and J. A. Harrington, "Optical properties of single-crystal sapphire fibers," Appl. Opt. **36**, 5934–5940 (1997).
8. Y. Matsuura, H. Hiraga, Y. Wang, Y. Kato, M. Miyagi, S. Abe, and S. Onodera, "Lensed-taper launching coupler for small-bore, infrared hollow fibers," Appl. Opt. **36**, 7818–7821 (1997).
9. R. George and J. A. Harrington, "Infrared transmissive, hollow plastic waveguides with inner Ag-AgI coatings," Appl. Opt. **44**, 6449–6455 (2005).
10. K. Iwai, M. Miyagi, Y. W. Shi, X. S. Zhu, and Y. Matsuura, "Infrared hollow fiber with a vitreous film as the dielectric inner coating layer," Opt. Lett. **32**, 3420–3422 (2007).
11. R. K. Nubling and J. A. Harrington, "Launch conditions and mode coupling in hollow-glass waveguides," Opt. Eng. **37**, 2454–2458 (1998).

12. Y. Matsuura, M. Saito, and M. Miyagi, "Loss characteristics of circular hollow fibers for incoherent infrared light," J. Opt. Soc. Am. A **6**, 423–427 (1989).
13. Y. W. Shi, K. Ito, L. Ma, T. Yoshida, Y. Matsuura, and M. Miyagi, "Fabrication of a polymer-coated silver hollow optical fiber with high performance," Appl. Opt. **45**, 6736–3670 (2006).
14. E. D. Palik, *Handbook of Optical Constants of Solids* (Academic, 1998), Vol. 1, pp. 749–763, Vol. 3, pp. 653–682.
15. J. A. Dobrowolski, Y. Guo, and T. Tiwald, "Toward perfect antireflection coatings. 3. Experimental results obtained with the use of Reststrahlen materials," Appl. Opt. **45**, 1555–1562 (2006).

Synchronous radiation with Er:YAG and Ho:YAG lasers for efficient ablation of hard tissues

Tomonori Watanabe,[1,*] Katsumasa Iwai,[2] Takashi Katagiri,[1] and Yuji Matsuura[3]

[1]*Tohoku University, Graduate school of Engineering, Sendai 980-8579, Japan*
[2]*Sendai National College of Technology, Sendai 989-3128, Japan*
[3]*Tohoku University, Graduate school of Biomedical Engineering, Sendai 980-8579, Japan*
**nabe-tom@ecei.tohoku.ac.jp*

Abstract: Er:YAG and Ho:YAG laser beams were combined to irradiate hard tissues to achieve highly efficient ablation with low laser power. The delay time between pulses of the two lasers was controlled to irradiate alumina ceramic balls used as hard tissue models. With optimized delay time, the combined laser beam perforated the sample 40% deeper than independent radiation by either an Er:YAG or Ho:YAG laser. An ultra-high-speed camera and an infrared thermography camera were used to observe and investigate the ablation mechanisms.

OCIS Codes: (170.0170) Medical optics and biotechnology; (170.1020) Ablation of tissue.

References and links

1. K. Matsuoka, S. Iida, M. Inoue, S. Yoshii, K. Arai, K. Tomiyasu, and S. Noda, "Endoscopic lithotripsy with the holmium:YAG laser," Lasers Surg. Med. **25**(5), 389–395 (1999).
2. M. K. Yiu, P. L. Liu, T. F. Yiu, and A. Y. T. Chan, "Clinical experience with holmium:YAG laser lithotripsy of ureteral calculi," Lasers Surg. Med. **19**(1), 103–106 (1996).
3. M. Grasso, "Experience with the holmium laser as an endoscopic lithotrite," Urology **48**(2), 199–206 (1996).
4. K. F. Chan, G. J. Vassar, T. J. Pfefer, J. M. H. Teichman, R. D. Glickman, S. T. Weintraub, and A. J. Welch, "Holmium:YAG laser lithotripsy: A dominant photothermal ablative mechanism with chemical decomposition of urinary calculi," Lasers Surg. Med. **25**(1), 22–37 (1999).
5. L. J. Walsh, "The current status of laser applications in dentistry," Aust. Dent. J. **48**(3), 146–155, quiz 198 (2003).
6. G. M. Hale, and M. R. Querry, "Optical constants of water in the 200-nm to 200-μm wavelength region," Appl. Opt. **12**(3), 555–563 (1973).
7. D. Fried, M. Zuerlein, J. D. B. Featherstone, W. Seka, C. Duhn, and S. M. McCormack, "IR laser ablation of dental enamel: mechanistic dependence on the primary absorber," Appl. Surf. Sci. **127-129**(1-2), 852–856 (1998).
8. H. Lee, H. W. Kang, J. M. H. Teichman, J. Oh, and A. J. Welch, "Urinary calculus fragmentation during Ho: YAG and Er:YAG lithotripsy," Lasers Surg. Med. **38**(1), 39–51 (2006).
9. K. F. Chan, B. Choi, G. Vargas, D. X. Hammer, B. Sorg, T. J. Pfefer, J. M. H. Teichman, A. J. Welch, and E. D. Jansen, "Free electron laser ablation of urinary calculi: an experimental study," IEEE J. Quantum Electron. **7**(6), 1022–1033 (2001).
10. P. Carmona, J. Bellanato, and E. Escolar, "Infrared and raman spectroscopy of urinary calculi: A review," Biospectroscopy **3**(5), 331–346 (1997).
11. D. Lezal, J. Pedlikova, and J. Horak, "GeO_2-PbO glassy system for infrared fibers for delivery of Er:YAG laser energy," J. Non-Cryst. Solids **196**, 178–182 (1996).
12. J. A. Harrington, *Infrared Fibers and Their Applications* (SPIE PRESS, 2004)
13. K. Itoh, K. Miura, I. Masuda, M. Iwakura, and T. Yamashita, "Low-loss fluorozirco-aluminate glass fiber," J. Non-Cryst. Solids **167**(1-2), 112–116 (1994).
14. Y. Yang, C. A. Chaney, and N. M. Fried, "Erbium:YAG laser lithotripsy using hybrid germanium/silica optical fibers," J. Endourol. **18**(9), 830–835 (2004).
15. S. Mohri, T. Kasai, Y. Abe, Y. W. Shi, Y. Matsuura, and M. Miyagi, "Optical properties of end-sealed hollow fibers," Appl. Opt. **41**(7), 1251–1255 (2002).
16. Y. W. Shi, K. Ito, L. Ma, T. Yoshida, Y. Matsuura, and M. Miyagi, "Fabrication of a polymer-coated silver hollow optical fiber with high performance," Appl. Opt. **45**(26), 6736–6740 (2006).
17. D. Fried, J. Ragadio, and A. Champion, "Residual heat deposition in dental enamel during IR laser ablation at 2.79, 2.94, 9.6, and 10.6 microm," Lasers Surg. Med. **29**(3), 221–229 (2001).
18. H. Pratisto, M. Ith, M. Frenz, and H. P. Weber, "Infrared multiwavelength laser system for establishing a surgical delivery path through water," Appl. Phys. Lett. **67**(14), 1963–1965 (1995).

#128212 - $15.00 USD Received 12 May 2010; revised 5 Jul 2010; accepted 27 Jul 2010; published 2 Aug 2010

19. H. Pratisto, M. Frenz, M. Ith, H. J. Altermatt, E. D. Jansen, and H. P. Weber, "Combination of fiber-guided pulsed erbium and holmium laser radiation for tissue ablation under water," Appl. Opt. **35**(19), 3328–3337 (1996).
20. J. Morita MFG, Co. http://www.jmorita-mfg.co.jp/html/jp_products_laser_erwin_adverl.htm.
21. Y. W. Shi, Y. Wang, Y. Abe, Y. Matsuura, M. Miyagi, S. Sato, M. Taniwaki, and H. Uyama, "Cyclic olefin polymer-coated silver hollow glass waveguides for the infrared," Appl. Opt. **37**(33), 7758–7762 (1998).
22. K. Iwai, Y. W. Shi, K. Nito, Y. Matsuura, T. Kasai, M. Miyagi, S. Saito, Y. Arai, N. Ioritani, Y. Okagami, M. Nemec, J. Sulc, H. Jelinkova, M. Zavoral, O. Kohler, and P. Drlik, "Erbium:YAG laser lithotripsy by use of a flexible hollow waveguide with an end-scaling cap," Appl. Opt. **42**(13), 2431–2435 (2003).
23. K. Nahen, and A. Vogel, "Plume dynamics and shielding by the ablation plume during Er:YAG laser ablation," J. Biomed. Opt. **7**(2), 165–178 (2002).
24. J. A. Izatt, N. D. Sankey, F. Partovi, M. Fitzmaurice, R. P. Rava, I. Itzkan, and M. S. Feld, "Ablation of calcified biological tissue using pulsed hydrogen fluoride laser radiation," IEEE J. Quantum Electron. **26**(12), 2261–2270 (1990).
25. K. L. Vodopyanov, "Saturation studies of H_2O and HDO near 3400 cm-1 using intense picosecond laser pulses," J. Chem. Phys. **94**(8), 5389–5393 (1991).
26. R. K. Shori, A. A. Walston, O. M. Stafsudd, D. Fried, and J. T. Walsh, "Quantification and Modeling of the Dynamic Changes in the Absorption Coefficient of Water at $\lambda = 2.94$ μm," IEEE J. Sel. Top. Quantum Electron. **7**(6), 959–970 (2001).

1. Introduction

Since the water that bio-tissues contain strongly absorbs infrared light, irradiation with infrared lasers has a strong effect on both hard and soft tissues and, therefore, is used in a variety of medical applications. In urological applications, such as treatment of enlarged prostate and fragmentation of urinary calculi, 2.1-μm wavelength Ho:YAG lasers are often used, and the laser light is delivered by common silica-glass fiberoptics in a thin endoscope to irradiate inside the human body [1–4]. In dental applications, 2.94-μm wavelength Er:YAG lasers are often used [5] because the wavelength coincides with a water absorption line [6], which enables highly efficient ablation of hydroxyapatite, which contains a large amount of water [7].

It has also been reported that more effective fragmentation of urinary calculi is possible with Er:YAG lasers [8] because the laser light is strongly absorbed by the calcium oxalate and magnesium ammonium phosphate in urinary calculi [9,10]. However, flexible silica-glass optical fibers cannot be used for delivery of Er:YAG lasers because of the absorption loss of silica in the 3-μm wavelength region. To solve this problem, optical fibers made of infrared transmission glasses such as germanium oxide [11] and fluoride glasses [12,13] have been proposed and developed for transmission of Er:YAG laser light. Although these glass fibers have low transmission losses, when transmitting high-powered lasers, they need special care on the input and output end surfaces because of fragileness of theses glasses. Also, for germanium-oxide glasses, the output end should be spliced to silica fiber tip when used in water [14]. In contrast, hollow optical fibers are robust and have high energy transmission capability and they are also useful for laser application in water by putting a glass cap on the distal end [15]. We have developed hollow optical fibers that deliver radiation of both the Er:YAG and the Ho:YAG lasers with high efficiency [16] and they enable simultaneous delivery of these two lasers.

To increase ablation speed for hard tissues such as teeth and calculi, radiation with laser pulses with a high average power becomes necessary. However, this also generates heat in the vicinity of the irradiated part [17] that could cause damage or pain. To improve ablation speed with infrared laser light, here we investigate effects of synchronous irradiation with Ho:YAG and Er:YAG lasers for more efficient hard tissue ablation. Pratisto, *et al*, reported that, in hard-tissue ablation in water, ablation effect of Er:YSGG laser light ($\lambda = 2.79$ μm) is enhanced more than twice when an Er:YSGG pulse is radiated after a Ho:YAG laser pulse with a delay time of 100 μs. This is because the Ho:YAG creates a vapor channel in water [18,19] and Er:YSGG transmits in the channel with a low absorption loss. In this case, the Ho:YAG works only for creating vapor channel in water and it has no direct effect on ablation. In this paper, we try increasing the ablation effect for tissues that have wet surface. We synchronously radiate Er:- and Ho:YAG lasers in air and show that both lasers have different ablation effects.

#128212 - $15.00 USD Received 12 May 2010; revised 5 Jul 2010; accepted 27 Jul 2010; published 2 Aug 2010

With a proper delay in these two laser pulses, these ablation effects enhance each other and give higher ablation effect.

2. Experimental setup

We used the experimental setup shown in Fig. 1 to irradiate a hard tissue model with light from two different lasers. Since we assume a laser system with a flexible hollow-optical fiber, we use a hollow fiber that is available in market [20]. The fiber also acts as an optic to irradiate a single small spot with combined beam of the two lasers. Ho:YAG (λ = 2.1 μm) and Er:YAG (λ = 2.94 μm) laser beams are combined with a dichroic mirror and the combined beam is focused by a f = 100 mm CaF_2 lens on the input end of a hollow optical fiber. The inner diameter of the fiber is 0.7 mm and the length is 30 cm. The inside surface of the hollow fiber is coated with silver and cyclic-olefin polymer (COP) thin film. The thickness of the COP is 0.3 μm so that the transmission losses for both Er:YAG and Ho:YAG lasers are reduced by the interference effect of the polymer film that acts as a reflection enhancement coating [21]. The transmission losses of the 30-cm long hollow optical fiber used in the experiment were 1.0 dB for Ho:YAG and 0.5 dB for Er:YAG laser light.

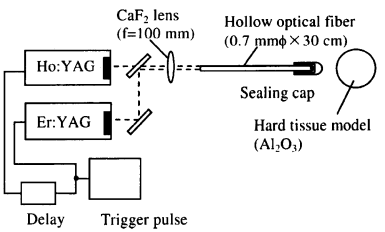

Fig. 1. Experimental setup with dual-wavelength laser.

The distal end of the hollow optical fiber is capped to protect the inside of the fiber from vapor and debris from the ablated tissues [15]. We used hemispheric silica glass caps [22]. The focusing effect of the caps enables highly efficient ablation due to the high energy intensity at the focal point. Figure 2 shows the laser beam diameters measured from burn patterns on thermal paper. The focal length of the cap is around 0.8 mm from the end surface for both lasers and the insertion loss is around 10% for the Ho:YAG and 15% for the Er:YAG laser. The difference is due to absorption by silica glass, which is slightly higher for Er:YAG laser light.

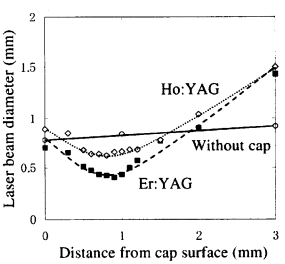

Fig. 2. Laser beam sizes measured from burn patterns.

#128212 - $15.00 USD Received 12 May 2010; revised 5 Jul 2010; accepted 27 Jul 2010; published 2 Aug 2010

The laser emission timing and repetition rates of the pulses of the two lasers are controlled by an external trigger source and a delay line. To evaluate the ablation capabilities, we radiated lasers onto alumina (Al_2O_3) ceramic balls used as a hard tissue model and human tooth samples. When alumina balls have been soaked in water for more than 24 hours, the water content and density are compatible to dentin and enamel of human tooth. We used a thermographic camera with 350-frame/sec of capture speed and an ultra-high-speed camera with 50,000-frame/sec capture speed to observe the ablation phenomena and investigate their mechanisms.

3. Experiment

3.1 Laser ablation

First, we irradiated alumina balls with Ho:YAG and Er:YAG laser pulses independently and measured the widths and depths of the ablated holes on the alumina balls. The diameters of the alumina balls were 4 to 6 mm. The balls had been soaked in water for more than 24 hours prior to the experiment and had water content of 5–10% by weight. The laser pulses used in the experiment for both lasers had 200 mJ of pulse energy, widths of 250 μs, and repetition rates of 3 Hz. The measured depths and widths as a function of number of pulses are shown in Fig. 3. Cross sections of the ablated holes after 30 pulses are shown in Fig. 4. The error bars show measurement accuracy.

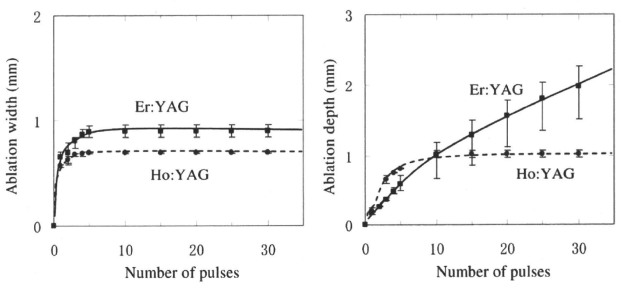

Fig. 3. Widths and depths of ablated holes as a function of number of laser pulses.

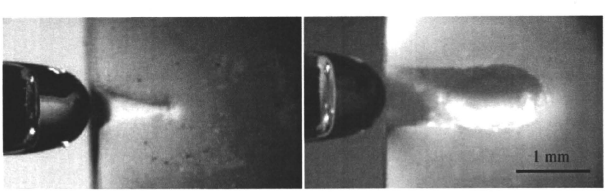

Fig. 4. Cross sections of alumina balls after ablation of 30 pulses.

Although the widths of the two lasers are comparable (Fig. 3), the depths are clearly different. When irradiated with the Ho:YAG, the depth saturated at large pulse numbers. This is because the energy density of the laser beam becomes lower than the ablation threshold of hard tissues when the beam spreads behind the focus spot. For the Er:YAG, in contrast, the

#128212 - $15.00 USD Received 12 May 2010; revised 5 Jul 2010; accepted 27 Jul 2010; published 2 Aug 2010

depth increases linearly with the number of pulses because the energy density of the laser beam always exceeds the ablation threshold due to the higher absorption coefficient in water for the Er:YAG laser light.

In the next experiment, to investigate the ablation capabilities, we measured the weight decrease of the alumina balls after laser ablation. The balls were fixed on the table and we irradiated the surface, randomly changing the irradiated spot without a water supply. The pulse widths were 250 μs for Ho:YAG and 300 μs for Er:YAG, and the irradiation time was 1 minute with a repetition rate of 10 Hz (600 pulses applied in total). Figure 5 shows the weight decreases of alumina balls as a function of pulse energy. The data show the average values of 10 measurements with different samples. As shown in Fig. 5, the weight linearly decreased with pulse energy and the ablation capability of the Er:YAG was two or three times higher than that of the Ho:YAG laser. This is apparently due to the difference of absorption in water of the two lasers.

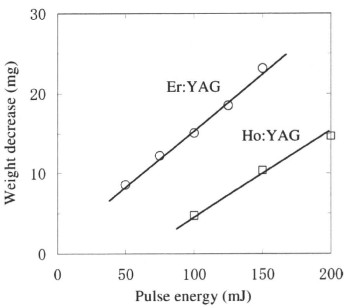

Fig. 5. Weight decreases of alumina balls after laser irradiation.

3.2 Ablation with two lasers

Next we investigated the ablation effect of synchronously irradiating with both lasers. We changed the delay time between the two lasers and observed the effect on the ablation of alumina balls. Both lasers had pulse energies of 100 mJ and pulse widths of 250 μs at a repetition rate of 3 Hz. We compared the ablation depths with those made by the Er:YAG alone with a pulse energy of 200 mJ.

Figure 6 shows cross sections of alumina balls after 40 pulses (20 pulses for each laser) with delay times of −100, 0, and 200 μs. Positive delay time means that the Ho:YAG was emitted before the Er:YAG. Figure 7 shows the depths of ablated holes after 10 pulses as a function of the delay time. It is clear that the depths are highly dependent on the delay time. When irradiated with a delay time of ± 500 μs or less, depths drastically changed with the delay. The smallest depth was obtained at the delay time of −100 μs, and the obtained depth was 25% smaller than those made by radiation with the Er:YAG laser alone. On the other hand, the deepest ablation was obtained at the delay time of 200–300 μs and the ablated hole was 40% deeper. In another experiments measuring weight decrease of the samples after laser radiation, we had results that are similar with the ones with ablation depth. Therefore we use ablation depth for evaluation of ablated volume in this paper. Figure 8 shows the measured depths ablated by a dual-wavelength laser with a delay time of 200 μs as a function of number of pulses. Data for radiation with the Er:YAG laser alone are also shown for comparison. Depths ablated by the dual-wavelength laser increased rapidly after only a few pulses.

#128212 - $15.00 USD Received 12 May 2010; revised 5 Jul 2010; accepted 27 Jul 2010; published 2 Aug 2010

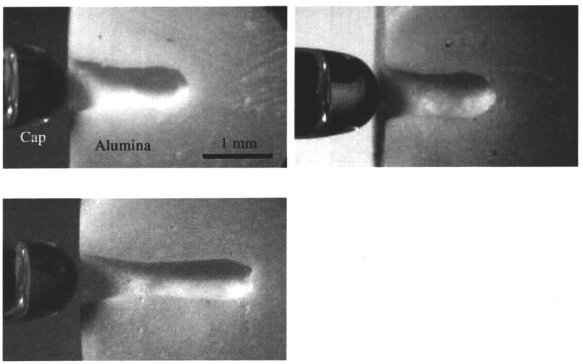

Fig. 6. Cross sections of alumina balls ablated by dual-wavelength laser with a delay time of (a) −100 μs, (b) no delay, (c) 200 μs.

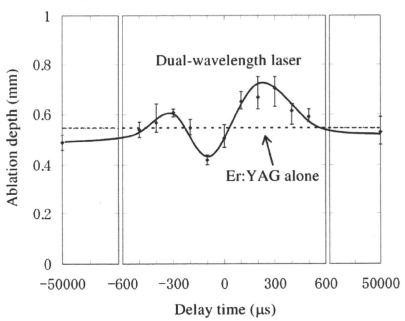

Fig. 7. Ablation depths of alumina balls as a function of delay time.

#128212 - $15.00 USD Received 12 May 2010; revised 5 Jul 2010; accepted 27 Jul 2010; published 2 Aug 2010

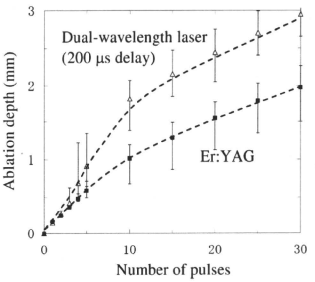

Fig. 8. Ablation depths of alumina balls as a function of number of pulses.

3.3 Observation

To investigate the ablation mechanism shown in Fig. 7, we observed the ablation phenomena using an ultra-high-speed camera. We irradiated alumina balls with laser pulses and recorded the moment of ablation at the surface at 50,000 frame/sec. Figures 9(a) and 9(b) show ablations with (a) Er:YAG and (b) Ho:YAG lasers alone. Figure 9(c) is the moment of an Er:YAG pulse that was shot 200 μs after a Ho:YAG pulse. When the sample was irradiated with Er:YAG laser light, powdery dust scattered from the surface immediately. This is because the laser energy was absorbed in the outermost surface of the ball. On the other hand, for the Ho:YAG laser, relatively large debris was scattered. The laser beam penetrated the ball and an explosive ablation occurred from the inside.

When a Ho:YAG pulse was shot after an Er:YAG, powdery dust generated by the Er:YAG blocked the Ho:YAG pulse [23,24]. As a result, the smallest depth was obtained with a delay time of −100 μs, as shown in Fig. 7. In contrast, when an Er:YAG pulse was emitted after a Ho:YAG pulse [Fig. 9(c)], large fragments were scattered. In this case, the Ho:YAG pulse gives ablation effect free from dust from ablation with the Er:YAG.

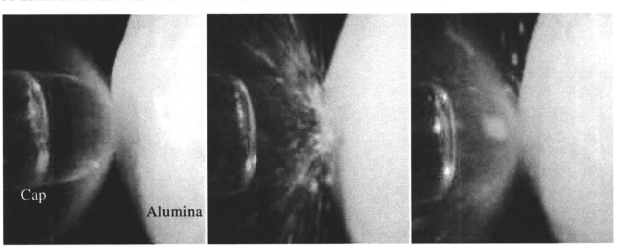

(a) Er:YAG (b) Ho:YAG (c) Ho:YAG and Er:YAG with a delay time of 200 μs

Fig. 9. Moment of ablation with Ho:YAG and Er:YAG lasers

Next, we used a thermographic camera to observe heat generation during ablation of the alumina balls. Figure 10 shows thermal images of cross sections of balls 3 ms after laser radiation. When the Er:YAG laser was used, heat generated from the laser beam stayed at the surface. In contrast, with the Ho:YAG laser, laser energy penetrated deeper and heat diffused over a large area. This was due to the difference of absorption coefficients and is one of the

#128212 - $15.00 USD Received 12 May 2010; revised 5 Jul 2010; accepted 27 Jul 2010; published 2 Aug 2010

reasons why the ablation with Ho:YAG occurred from the inside as shown in Fig. 9(b). At the optimum condition in Fig. 7, where the Er:YAG emitted 200 μs after the Ho:YAG, the heat was generated in a deeper area before the Er:YAG pulse. This decreased the absorption coefficient of water and the Er:YAG laser beam penetrated deeper into the ball, which led to ablation from within the ball.

From these results, it is seen that the Ho:YAG laser apparently plays a part in ablation. Ho:YAG laser light penetrates deeper into the tissue and causes ablation from deeper area in contrast to Er:YAG laser light that is strongly absorbed and ablates the tissue from the outmost surface. When these two lasers are simultaneously radiated, ablation from the surface and deeper area occur in the same time. Furthermore, they have synergetic effects in ablation. Heat generated by the Ho:YAG pulse that is radiated on ahead decreases the absorption coefficient of water at 2.94-μm wavelength [25,26], and the Er:YAG can penetrate deeper and ablate the tissue from deeper area. However, this synergistic effect is limited by debris induced by laser light. If the debris on the laser path can be perfectly removed, we can irradiate two lasers just simultaneously to the tissue, which will lead to stronger ablation effect. We are now trying to remove the debris by spraying water during the ablation and the result will be reported elsewhere.

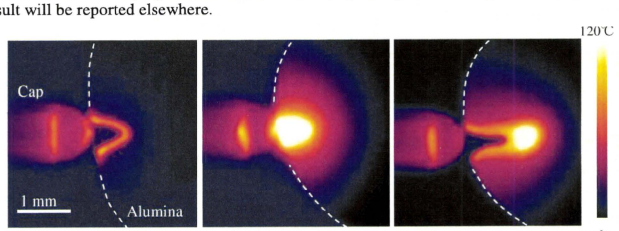

Fig. 10. Thermal images of cross sections of balls after laser pulse irradiation.

3.4 Dental ablation

We also applied dual-wavelength laser radiation to human teeth. Human teeth were sliced into 0.3-mm-thick pieces and soaked in water before the experiment. The same ablation experiments as above were performed, and we used an ultra-high-speed camera to observe the ablation phenomena on the dentin surface. Figures 11(a) and 11(b) show the ablation phenomena with (a) Er:YAG and (b) Ho:YAG lasers alone. Figure 11(c) is the moment of an Er:YAG pulse shot 200 μs after the Ho:YAG. This ablation was similar to the one observed for alumina balls (compare to Fig. 9), and there was also a synchronous radiation effect for the two lasers.

#128212 - $15.00 USD Received 12 May 2010; revised 5 Jul 2010; accepted 27 Jul 2010; published 2 Aug 2010

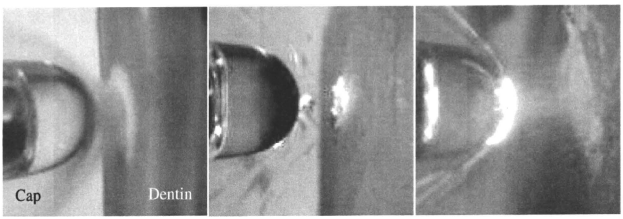

(a) Er:YAG (b) Ho:YAG (c) Ho:YAG and Er:YAG with a delay time of 200 μs

Fig. 11. Moment of ablation of dentin with Ho:YAG and Er:YAG lasers.

Figure 12 shows a cross section of human dentin after 5 pulses of laser irradiation with a repetition rate of 3 Hz. Ablation effects for the tooth samples were similar to those for the alumina balls. At the optimum condition described above, we obtained 25% deeper ablation than in the tooth irradiated with Er:YAG only.

We used an optical microscope to investigate the surface condition of dental tissues after laser ablation. Figure 13 shows the surface of the dentin after sole radiation of Ho:YAG and Er:YAG, and dual-wavelength laser radiation of these. With the Ho:YAG, the surface is thermally damaged and carbonized in contrast to the surface radiated with the Er:YAG that has no damage. When irradiated with combination of these two lasers, the surface had a little thermal damage that is due to heat generated by the Ho:YAG. Since the surface of the dental tissue was not cooled in this experiment, the thermal damage will be largely reduced by applying water cooling.

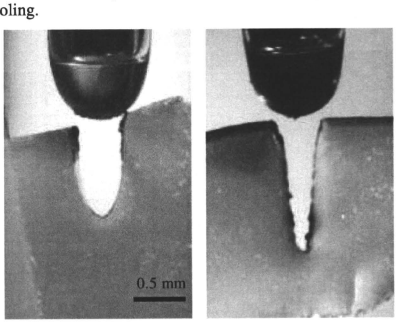

(a) Er:YAG (200 mJ) (b) Ho:YAG (100 mJ) and Er:YAG(100 mJ, 200 μs delay)

Fig. 12. Cross section of human dentin after laser irradiation.

#128212 - $15.00 USD Received 12 May 2010; revised 5 Jul 2010; accepted 27 Jul 2010; published 2 Aug 2010

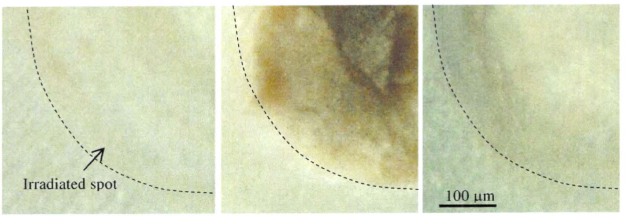

(a) Er:YAG (b) Ho:YAG (c) Ho:YAG and Er:YAG with a delay time of 200 μs

Fig. 13. Surface of dentin after laser ablation.

4. Conclusion

Laser ablation experiments were performed on hard tissues using a combined beam of Ho:YAG and Er:YAG laser light. Alumina balls were used as a hard-tissue model and ablation phenomena were observed with an ultra-high-speed camera. The two lasers had different ablation effects due to the different absorption coefficients in water contained in the tissues. When the two lasers were combined to irradiate the sample, ablation capabilities were highly dependent on the delay time between the pulses of the two lasers. When the Er:YAG laser radiated 200 μs after the Ho:YAG, the ablated hole was 40% deeper.

With combination of these two lasers, ablation from the surface that is with Er:YAG and deeper area with Ho:YAG occur in the same time. Furthermore, heat generated by the Ho:YAG pulse that is radiated on ahead decreases the absorption coefficient of water at the Er:YAG wavelength. Then the Er:YAG can penetrate deeper and ablate the tissue from deeper area. The same ablation effects were seen on human dentin; sharp, deep holes were ablated in the dentin at the optimum condition.

#128212 - $15.00 USD Received 12 May 2010; revised 5 Jul 2010; accepted 27 Jul 2010; published 2 Aug 2010

I64a III 006

CO_2 レーザー光伝送用細径金属プローブ

Small-diameter Metallic Probe for CO_2 Laser Light Transmission

岩井克全[A]，○本郷晃史[B]，高久裕之[A]，宮城光信[A,]，石山純一[A]，石芸尉[C]
([A]仙台高等専門学校，[B]日立電線，[C]復旦大学)
Katsumasa Iwai[A]，○Akihito Hongo[B]，Hiroyuki Takaku[A]，Mitsunobu Miyagi[A]，Jun-ichi Ishiyama[A]，Yi-Wei Shi[C]
([A]Sendai National College of Technology，[B]Hitachi Cable Ltd.，[C]Fudan University)

1. はじめに

環状オレフィンポリマー（COP）やヨウ化銀（AgI）など赤外領域において透明な誘電体薄膜を内装した金属中空ファイバは，所望の赤外光を低損失で伝送できる。今回，CO_2 レーザー光伝送用として内径 0.375mm の細径な金属プローブを試作したので，その光学特性を報告する。

2. AgI 内装銀クラッド細径金属プローブの構造

図 1 に試作した AgI 内装銀クラッドステンレス管（AgI/Ag/SUS）の断面写真を示す。AgI/Ag/SUS 管は，内面研磨した銀クラッドステンレス管（Ag/SUS）[1] の銀の内壁表皮層をヨウ素化して AgI 層を形成したもので，内径 0.375mm、外径 0.6mm、長さ 50mm である。

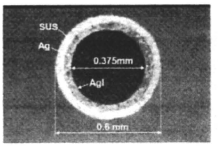

図 1　AgI/Ag/SUS プローブの断面写真

3. 金属プローブの光学特性

図 2 に、Ag/SUS 管と、これを用いた AgI/Ag/SUS 管の損失波長特性を示す。ここでニクロム光源と赤外分光器により各金属プローブの透過出力を測定し、長さ 18mm の同径 Ag/SUS 管との出力比より相対損失とした。相対損失が負となる波長域は、長さ 50mm の AgI/Ag/SUS の方が長さ 18mm の Ag/SUS よりも低損失であることを示す。損失ピークの波長より、AgI 層の膜厚は約 0.68 μ m と見積られる。CO_2 レーザー光をレンズで集光し入射したときの透過率は、50mm の長さで AgI/Ag/SUS が 88%、Ag/SUS が 33%であった。

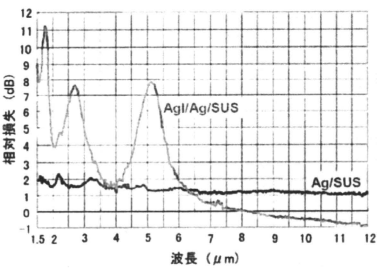

図 2　Ag/SUS 及び AgI/Ag/SUS の損失波長特性

4. まとめ

赤外光を低損失で伝送できる AgI/Ag/SUS 構造の細径金属プローブを試作した。歯科用レーザー治療器に用いられる先端ニードルチップや微小領域の放射温度計測用プローブとして有用と思われる。

参考文献 1) A. Hongo et al., Chinese Opt. Lett., **5**, S70-S72 (2007).

I64a III 007

各種金属管を用いた COP 内装金属中空ファイバの伝送特性

Transmission Properties of COP-Coated Various Metallic Hollow Fiber

○岩井克全[A]，本郷晃史[B]，高久裕之[A]，宮城光信[A,C]，石山純一[C]，石芸尉[D]
([A]仙台電波工業高等専門学校，[B]日立電線，[C]宮城工業高等専門学校，[D]復旦大学)
Katsumasa Iwai[A]，Akihito Hongo[B]，Hiroyuki Takaku[A]，Mitsunobu Miyagi[A,C]，Jun-ichi Ishiyama[C]，Yi-Wei Shi[D]
([A]Sendai National College of Technology，[B]Hitachi Cable Ltd.，[C]Miyagi National College of Technology，[D]Fudan University)

1. はじめに

耳鼻咽喉科治療の CO_2 レーザー（発振波長 10.6 μm)用プローブとして，金属管を母材とした中空ファイバは，機械的強度に優れていることから多く用いられ，その伝送損失の低減が望まれている．本研究では，金属中空ファイバの低損失化を図る目的で，内装材料として環状オレフィンポリマー（COP)[1]を用い，各種 COP 内装金属中空ファイバを製作したので，その伝送特性について述べる．

2. COP 内装金属中空ファイバの損失波長特性

図 1 に，各種 COP 内装金属中空ファイバの損失波長特性を示す．COP 内装銀クラッドステンレス管 (COP/Ag/SUS)，金メッキステンレス管 (COP/Au/SUS)，ステンレス管 (COP/SUS)，そして石英チューブを母材とした銀中空ファイバ (COP/Ag/SiO_2)の COP 膜厚は，それぞれ 0.96 μm, 0.98 μm, 0.96 μm, 0.85 μm であり，CO_2 レーザー光伝送に適した膜厚を成膜した．波長 10.6 μm において，COP/Ag/SUS と COP/Au/SUS は，COP/Ag/SiO_2 と同程度の損失となった．

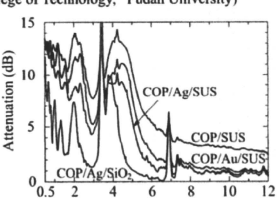

図 1　各種 COP 内装金属中空ファイバの損失波長特性

3. 金属中空ファイバの CO_2 レーザー光伝送特性

表 1に，各種金属中空ファイバの CO_2 レーザー光伝送特性を示す．結果から，COP を 1 層内装するだけで，伝送損失の低減化は極めて大きいと思われる．また，COP/Ag/SUS と COP/Au/SUS の損失値は 0.2 dB で，COP/Ag/SiO_2 と同程度の低損失値を示した．COP/Au/SUS と COP/Ag/SUS の内径は，それぞれ 0.94 mm と 0.75 mm と異なるため，同径で比較すると COP/Ag/SUS の方が透過率がよいと思われる．

表 1　各種金属中空ファイバの CO_2 レーザー光伝送特性

Material	Size (mm)			Loss (dB)
	ID	OD	L	
SUS	0.94	1.2	285	3.7
Au/SUS	0.94	1.2	285	2.1
Ag/SUS	0.75	1.2	280	1.7
Ag/SiO_2	0.75	0.9	280	1.8
COP/SUS	0.94	1.2	285	0.6
COP/Au/SUS	0.94	1.2	285	0.2
COP/Ag/SUS	0.75	1.2	280	0.2
COP/Ag/SiO_2	0.75	0.9	280	0.1

4. まとめ

各種金属および COP を内装した金属中空ファイバの伝送損失を比較した．その結果，COP に接する金属は銀が最も低損失になることを確認した．

参考文献 1) Y. W. Shi et al., Appl. Opt. , **37**, 7758-7762 (1998).

AgI 内装銀クラッド SUS 中空ファイバの AgI 膜厚制御

Thickness Control of AgI-Film in AgI/Ag Hollow Silver-Cladding-Stainless Pipe

岩井　克全[*1]　高久　裕之[*1]　宮城　光信[*1]　石山　純一[*1]　本郷　晃史[*2]　石　芸尉[*3]
Katsumasa Iwai　Hiroyuki Takaku　Mitsunobu Miyagi　Jun-ichi Ishiyama　Akihito Hongo　Yi-Wei Shi

[*1]仙台高等専門学校 Sendai National College of Tech.
[*2]日立電線 Hitachi Cable Ltd.
[*3]復旦大学 Fudan Univ.

1. はじめに

CO_2 レーザ光 (波長 10.6 μm)の高エネルギー伝送を行う時、ヨウ化銀内装銀(AgI/Ag)中空ファイバが有効である [1]。その際、低損失に伝送させるため、AgI 膜厚を制御し、ファイバ内面に最適膜厚を一様に内装する技術が必要である。

本研究では、銀クラッドステンレス管を用いた AgI/Ag (AgI/Ag/SUS)中空ファイバの AgI 膜厚制御について述べる。

2. AgI/Ag/SUS 中空ファイバの AgI 膜厚の増加

図 1 に、AgI/Ag/SUS 中空ファイバの構造図を示す。内面研磨した銀クラッドステンレス管 (内径 0.75 mm、外径 1.2 mm、長さ 280 mm)に、ヨウ素液を送液し、AgI 層を形成する。CO_2 レーザ光伝送に最適な AgI 膜厚は、0.89 μm であり、銀層の厚さは 100 μm 程度あるので、十分 AgI 層を形成できる。

図 2 に、ヨウ素液の送液回数に対する AgI/Ag/SUS 中空ファイバの損失波長特性を示す。図中の数値は、送液回数である。1 回の送液工程は、シリンジポンプを用いてヨウ素液 (濃度 1 %)を充填し、120 秒間保持した後、溶液を排出し、空気を流して乾燥している。充填と排出に要する時間は、およそ 4 秒である。明確な損失ピークが見られ、このピークの位置は、内装誘電体の膜厚に依存し、長波長側ほど膜厚は厚い。送液回数 2 回、3 回、4 回の AgI 膜厚は、それぞれ 0.59 μm、0.72 μm、0.81 μm となり、1 回の送液で 0.1 μm 程度、膜厚が増加することが分った。

3. AgI/Ag/SUS 中空ファイバの AgI 膜厚の減少

銀のヨウ化反応時間によって AgI 層の膜厚を制御できるが、一旦形成した AgI 層をチオ硫酸ナトリウムによりエッチング除去することができる。図 3 に、チオ硫酸ナトリウム水溶液の送液に対する AgI/Ag/SUS 中空ファイバの損失波長特性を示す。送液前の AgI 膜厚は、0.86 μm である。送液速度は 3cm/sec で行った。図中の A の送液条件は、濃度 0.1 ml/L で、送液時間 30 秒であり、B は濃度 0.05 ml/L、送液時間 300 秒、C は濃度 0.1 ml/L、送液時間 180 秒である。A、B、C の条件により、AgI 膜厚は、それぞれ 0.73 μm、0.72 μm、0.59 μm と減少した。0.05 ml/L の濃度を用いると、膜厚の微小な減少ができ、濃度 0.1 ml/L の時、送液時間を 30 秒以上にしても、膜厚の減少量は変わらないことが分った。

4. まとめ

AgI/Ag/SUS 中空ファイバの AgI 膜厚制御を試みた。AgI 膜厚の均一性を保ちつつ、微小な膜厚制御に成功した。

参考文献

1) Y. Matsuura et al., Appl. Opt. 35, 5395-5397 (1996).

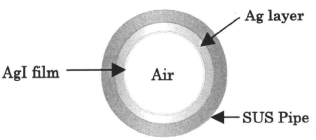

図 1　AgI 内装銀クラッド SUS 中空ファイバ
但し、中空コア径 0.75 mm、長さ 280 mm

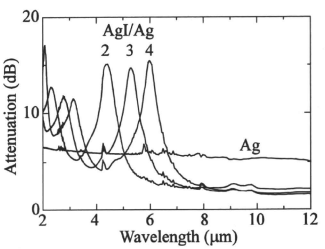

図 2　ヨウ素液の送液に対する AgI/Ag/SUS 中空ファイバ (0.75 mmϕ×280 mm)の損失波長特性
但し、図中の値は、送液回数、1 回の送液は、濃度 1%で充填時間 120 秒

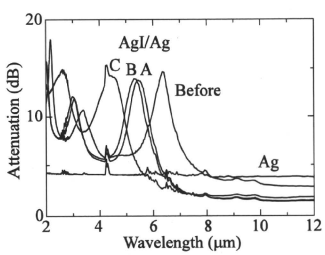

図 3　チオ硫酸ナトリウム水溶液の送液に対する AgI/Ag/SUS 中空ファイバ (0.75 mmϕ×280 mm)の損失波長特性
但し、図中の A は濃度 0.1 mol/L、送液時間 30 秒、B は濃度 0.05 mol/L、送液時間 300 秒、C は濃度 0.1 mol/L、送液時間 180 秒

2B11

中空ファイバにおける環状オレフィンポリマー成膜法の改善
- COP 溶液の濃度に対する粘度特性 -

○岩井克全*，高久裕之*，宮城光信**，石　芸尉***
*仙台高等専門学校，**東北学院大学，***復旦大学

1. はじめに

環状オレフィンポリマー (COP)内装銀中空ファイバの効率良い製作[1]として、簡易な COP 成膜法が求められているが、従来の COP 溶液の濃度と送液速度による成膜条件では、十分ではない。そこで、COP 溶液の使用期間を大幅に延ばすために、COP 溶液の粘度を成膜条件として検討する。

2. COP 保管日数に対する粘度と膜厚特性

COP(粒)の溶剤にシクロヘキサンを用い、攪拌を 3 日程度行い、その後、孔径 0.2 μm のフィルタでろ過し、COP 溶液 (濃度 8wt%)を製作した。COP 溶液 (約 10 ml)を容量 20 ml のガラス瓶に入れ、蓋と瓶の間にアルミシートを挟み、蓋と瓶をパラフィンフィルムでシーリングして保管した。溶液温度は約 20℃とし、粘度の測定方式は、SV 型 (音叉型振動式)粘度計を用いた。

図 1 に中空ファイバへの COP 膜のコーティング装置を示す。銀中空ファイバ (内径 0.7 mm、長さ 1 m)に COP 溶液 (8 wt%)を、マイクロチューブポンプを用い、送液速度 3 cm/min で送液し、送液後、窒素 (100 ml/min)を流しながら室温で 30 分乾燥を行った。

図 2 に COP 溶液 (8 wt%)の保管日数に対する COP 溶液の粘度と内径 0.7 mm 銀中空ファイバに成膜した際の COP 膜厚特性を示す。保管期間 4 日程度で、粘度は安定した。これはろ過後に残っていた COP (0.2 μm 以下の粒)が溶剤に溶け切ったためと思われる。14 日経過してもほとんど粘度は変化しないことから、今回用いた COP 溶液の保管方法は有効と思われる。COP 溶液の粘度の増加により、COP 膜厚も増加することが確認された。

3. COP 溶液の濃度に対する粘度特性

図 3 に赤外伝送路用 COP 膜の形成に用いる COP 溶液の濃度 (8 wt%～12 wt%)に対する粘度特性を示す。各濃度の COP 溶液 (約 15 ml)をそれぞれ 3 個ずつ製作し、測定を行った。濃度 10 wt%以上では、粘度の測定値は大きく変動することが分った。これは濃度が高いと、COP 溶液表面に薄膜が形成され易く、そのため測定値が変動したためと思われる。

4. まとめ

COP 溶液の粘度を用いて、COP 膜の成膜条件について検討を行った。COP 溶液の保管日数、濃度に対する COP 溶液の粘度特性を明らかにした。

参考文献

1) K. Iwai, Y. W. Shi, M. Miyagi and Y. Matsuura : Opt. & Laser Technol. 39, 8, 1528 (2007).

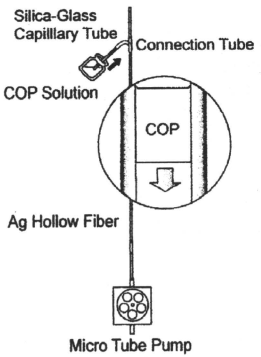

図 1　中空ファイバへの COP 送液法

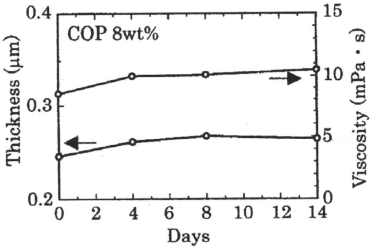

図 2　COP 溶液 (8 wt%) の保管日数に対する粘度と COP 膜厚 (内径 0.7 mm 中空ファイバに成膜)

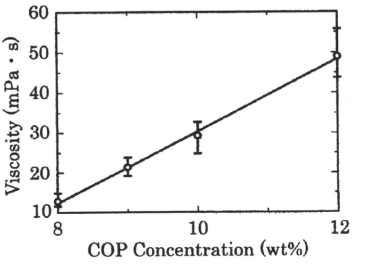

図 3　COP 溶液の濃度に対する粘度特性

内径 50 μm 銀中空ファイバの伝送特性の改善

Improvement of Transmission Properties for 50-μm bore Silver Hollow Fiber

岩井　克全[*1]　元木　沙綾[*1]　宮城　光信[*2]　石　芸尉[*3]
Katsumasa Iwai　Saaya Motoki　Mitsunobu Miyagi　Yi-Wei Shi

[*1] 仙台高等専門学校　[*2] 東北学院　[*3] 復旦大学　情報科学工学部
Sendai National College of Tech.　School Corporation of Tohoku Gakuin　School of Information Science and Eng., Fudan Univ.

1. はじめに

筆者らは、中空ファイバの医療応用範囲を歯科内視鏡等の低侵襲治療に広げるために内径 50 μm 中空ファイバの製作を行ってきた[1]。本研究では、内径 50 μm 中空ファイバを製作するための課題である低損失な銀中空ファイバの製作法について改善を試みた。

2. 製作と特性評価

銀膜の形成は銀鏡反応により行う。図 1 に内径 50 μm 銀中空ファイバの製作装置を示す。中空ファイバの内径が細くなると銀鏡反応溶液の流速が低下し、下流付近のファイバ内面には粗い銀が形成されてしまう。そこで、石英ガラスキャピラリ(内径 50 μm、外径 150 μm、長さ 50 cm)を 300 本束ねたバンドルを製作し、断面積を大きくすることで、流量の増加 を行った。流量については、これまで製作した内径 320 μm 銀中空ファイバの製作条件から、10 ml/min 程度を目標とする。

目標の流量を達成するために、バンドル化した石英ガラスキャピラリの本数に対する流量の測定を行った。結果を図 2 に示す。4800 本以上では流量の増加量は少なくなり、これは本数が増えるとバンドルの並列接続数も増加するため、並列接続する際に用いる接続チューブ長が長くなることで、溶液が流れ難くなったためと思われる。石英ガラスキャピラリを 300 本束ねたバンドルを 32 本並列接続することにより、11.2 ml/min を実現した。この装置で銀鏡反応を行い、銀鏡時間 7 分、後処理をした後、窒素を流しながら室温乾燥を 30 分間行った。

図 3 に製作した内径 50 μm 中空ファイバ (長さ 10 cm)の可視 - 近赤外波長帯における損失波長スペクトル(FWHM10.6 ° のガウスビームで励振)を示す。流量約 11 ml/min の条件で製作した銀中空ファイバは、波長 1 μm において、10 dB～13 dB となり、最大値と最小値の差が 3 dB 程度となり、ばらつきを抑えることが出来た。この装置で十分低損失なファイバを製作できることが分かった。

3. まとめ

内径 50 μm、長さ 10 cm の銀中空ファイバの製作において、銀鏡反応における溶液流量を 10 ml/min 以上に改善することで伝送特性のばらつきを抑制し、波長 1 μm において 10 dB 程度の超細径銀中空ファイバの製作に成功した。

参考文献

1) 阿部、庄子、岩井、宮城、石、平成 21 年度電気関係学会東北支部連合大会、2D09 (2009).

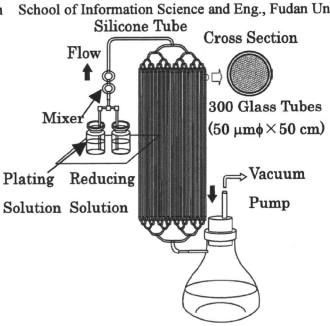

図 1　超細径銀中空ファイバ製作装置

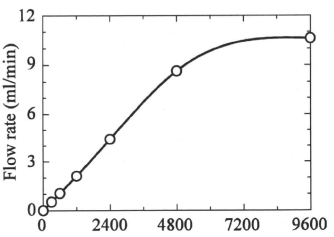

図 2　内径 50 μm ガラスキャピラリの本数に対する蒸留水の流量

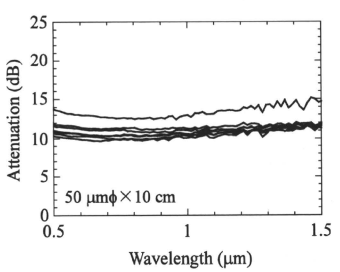

図 3　内径 50 μm 銀中空ファイバの損失波長スペクトル(FWHM10.6 °のガウスビームで励振)